30 January 2003

The complete Z-diagram of LMC X–2

A. P. Smale[1], J. Homan[2], and E. Kuulkers[3]

ABSTRACT

We present results from four *Rossi X-ray Timing Explorer (RXTE)* observations of the bright low mass X-ray binary LMC X–2. During these observations, which span a year and include over 160 hrs of data, the source exhibits clear evolution through three branches on its hardness-intensity and color-color diagrams, consistent with the flaring, normal, and horizontal branches (FB, NB, HB) of a Z-source, and remarkably similar to Z-tracks derived for GX 17+2, Sco X–1 and GX 349+2. LMC X–2 was observed in the FB, NB, and HB for roughly 30%, 40%, and 30% respectively of the total time covered. The source traces out the full extent of the Z in $\sim$1 day, and the Z-track shows evidence for secular shifts on a timescale in excess of a few days. Although the count rate of LMC X–2 is low compared with the other known Z-sources due to its greater distance, the power density spectra selected by branch show very-low-frequency noise characteristics at least consistent with those from other Z-sources. We thus confirm the identification of LMC X–2 as a Z-source, the first identified outside our Galaxy.

Subject headings: accretion, accretion disks — stars: individual (LMC X–2) — stars: neutron — stars: binaries: close — X-rays: stars

1. Introduction

Accreting low mass X-ray binaries (LMXBs) have been divided into two groups based on their broadband spectral and timing properties. The six currently-known Z-sources,

[1]USRA Research Scientist, Laboratory for High Energy Astrophysics, Code 660.1, NASA/Goddard Space Flight Center, Greenbelt, MD 20771; alan@osiris.gsfc.nasa.gov

[2]Osservatorio Astronomico di Brera, Via E. Bianchi 46, 23807 Merate LC, Italy; homan@merate.mi.astro.it

[3]ESA-ESTEC, Science Operations & Data Systems Division, SCI-SDG, Keplerlaan 1, 2201 AZ Noordwijk, The Netherlands; ekuulker@estsa2.estec.esa.nl

named for the three-branched shape they describe on a diagram of 'hard' color versus 'soft' color, are Sco X–1, GX 17+2, GX 349+2 (=Sco X–2), Cyg X–2, GX 340+0, and GX 5–1 (Hasinger & van der Klis 1989). From the top down, the three branches of the Z are known as the horizontal branch (HB), normal branch (NB), and flaring branch (FB), and the power spectra of these sources generally show several types of quasi-periodic oscillations (QPOs) and noise components (e.g. van der Klis 1995) based on the position of the source on the Z. When bright, Cir X–1 also shows Z-source characteristics (Shirey et al. 1998; Shirey, Bradt & Levine 1999). The mass accretion rate is generally thought to increase as the source passes from the HB, through the NB, to the FB. Motion along the Z is continuous, with no jumps from branch to branch.

The remainder of the bright Galactic LMXBs are known as 'atoll' sources and describe a simpler curved shape on a color-color diagram, generally consisting of a band of points, plus one or more 'islands'. Atoll sources that display a range of intensities approaching two orders of magnitude may reveal a three-band shape (Muno, Remillard & Chakrabarty 2002), but on much longer timescales (∼weeks–months) than the Z-source tracks (∼hours–days). The difference in their nature implies that Z- and atoll-sources differ in their evolutionary history (Hasinger & van der Klis 1989).

A previous *RXTE* observation of LMC X–2 in 1997 December showed timing and spectral characteristics more typical of a Z-source in its flaring branch than of an atoll source in any intensity state (Smale & Kuulkers 2000). Based on these findings and the high intrinsic luminosity of LMC X–2, which historically spans 0.4–2.0L_{Edd} for reasonable estimates of the neutron star mass, we then provisionally reclassified LMC X–2 as a Z-source, the seventh known and the first to be detected beyond our Galaxy. Here we present extensive additional *RXTE* data from LMC X–2 in which the source convincingly traces out all three branches in its hardness-intensity and color-color diagrams, confirming its Z-source identification.

2. Observations and Analysis

LMC X–2 was observed using the *Rossi X-ray Timing Explorer (RXTE)* (Bradt, Rothschild, & Swank 1993) on four occasions during 2001–2002 (Table 1), for a total on-source good time of 600 ksec. The data presented here were collected by the proportional counter array (PCA) instrument using the Standard 2 and Good Xenon configurations, with time resolutions of 16 s and 0.95 μs respectively. The PCA consists of five Xe proportional counter units (PCUs) numbered 0–4, with a combined total effective area of about 6500 cm^2 (Jahoda et al. 1996). PCUs 0 and 2 were reliably on during all observations, and for consistency across the whole dataset we utilized data from just these PCUs for the generation of light

curves and color-color diagrams. To maximize the statistics, for our timing analysis we used data from all available PCUs.

The background-subtracted light curves for each observation presented in Figure 1 include LMC X–2 data from the energy range 2.5–18.5 keV. To construct the hardness-intensity diagrams (HID) and color-color (CD) diagrams also shown, we followed conventional practice in the field and defined several "colors", representing the ratios of count rates in two different energy bands. The "overall" color is the ratio of the 6.5–18.5 keV band to the 2.5–6.5 keV band, and the HID are plots of this overall color against the 2.5–18.5 keV source intensity. CD are plots of the "hard" color [(9.8–18.5 keV)/(6.5–9.8 keV] against the "soft" color [(4.5–6.5 keV)/(2.5–4.5 keV)].

3. Results

3.1. Light curves and colors

In Figure 1a we show the background-subtracted light curve for the 2001 February observation. Two episodes of major flaring are observed, during which the source intensity almost doubles. Preceding this flaring behavior are two sections of low-level variability, and following the second series of flares the source settles into an interval of slightly higher, almost constant count rate.

Figure 1a also shows the HID and CD derived for these data using the colors defined in the previous section. These diagrams bear a remarkable resemblance to those seen in e.g. GX 17+2 (Hasinger & van der Klis 1989, Kuulkers et al. 1997, Homan et al. 2002) and show very little similarity with those seen from atoll sources (e.g. Hasinger & van der Klis 1989, Prins & van der Klis 1997, Wijnands et al. 1998). Dividing the data into sections of

Table 1. OBSERVATIONS OF LMC X–2

Obs.	ObsID	Date/Time (UT)	Good Time
1	50041-01-01-*	2001 Feb 10/17:35 – Feb 14/03:28	149 ksec
2	60017-01-01-*	2001 Aug 30/12:12 – Sep 03/02:40	143 ksec
3	60017-01-02-*	2001 Dec 13/22:22 – Dec 16/23:27	139 ksec
4	60017-01-03-*	2002 Feb 01/02:56 – Feb 06/16:21	149 ksec

a few hundred seconds each and examining the correlated variability in each section we can identify the three characteristic branches of the Z; during the 83-hr span of the observation, LMC X–2 moves in turn through the NB, FB, NB, FB, NB, and HB.

Subsequent panels of Figure 1 show the light curves, HIDs, and CDs for the 2001 August, 2001 December, and 2002 February observations of LMC X–2. The source spends almost all of the second observation on the FB, with some data defining the NB/FB vertex. The third observation contains data from the NB and part of the HB, while the fourth observation provides evidence for strong evolution along the HB, with a swift (~few thousand second) excursion through the NB and a brief flare lasting ~10,000s. No bursts were detected during any of the observations.

In Figure 2 we present the HID and CD for all four LMC X–2 observations combined. The combined CD (Fig. 2b) is a simple superposition of the data from all four of the individual CDs in Figure 1. However, a small secular shift in the position of the HB/NB and NB/FB vertices is evident in the individual HIDs, and we thus subtracted constants of 0.045 and 0.01 from the colors given in Fig. 1b and Fig. 1d respectively, prior to the superposition. (Failure to do this results in a combined HID with an unrealistically broad and skewed Normal branch, and the appearance of two FBs.)

To assess whether these shifts were intrinsic to the source or to the *RXTE* PCA detectors, we analyzed data from the Crab obtained close in time to our LMC X–2 observations. Extraction of the Crab CD and HID, using the same channels as those used for LMC X–2, showed that the gradual gain change of the PCA detectors over the span of our observations could account for a variation of less than 1% in the derived colors. The secular shifts in the HIDs of LMC X–2 amount to 10% and 2.5% changes, greatly in excess of this. We thus conclude that the source itself displayed intrinsic shifts, similar to the secular shifts seen in other Z-sources (see Discussion).

3.2. Variability analysis

For our power spectral analysis data were divided into three selections representing the HB, NB, and FB, based on their position along the Z-track in the CD and HID. Power spectra were created from the high-time-resolution Good Xenon mode data covering 2–21 keV, using standard Fast Fourier Transform techniques over the frequency range 1/128–512 Hz. No narrow features were present in the power density spectra, and each could be well fit (χ^2_ν=1.06–1.21) with a single power law with shape P $\propto \nu^{-\gamma}$, representing very low frequency noise (VLFN). The low count rate of the source does not allow us to parameterize

high-frequency noise (HFN) or perform a sensitive search for QPOs.

The horizontal branch spectrum (Figure 3a) was constructed using 170 ksec of data, and the VLFN component has a power law index of γ=0.60±0.05 and an rms amplitude of 1.9±0.1% (0.01–1 Hz). For the normal branch spectrum (Fig. 3b) 229 ksec of data were used, and the power law component has γ=0.90±0.05, rms=1.8±0.1%. The flaring branch spectrum uses 161 ksec of data, and has γ=1.33±0.03, rms=3.20±0.05%. Sections of data totaling 40 ksec were excluded from the analysis due to ambiguity about which branch they fell into; datapoints obtained around the NB/FB vertex are particularly difficult to assign.

For the data obtained on the NB we detected no QPOs, and and derive upper limits of 1% rms for oscillations with parameters typical of Z-sources (e.g. centroid position of ∼6 Hz, FWHM 2 Hz). For the FB data we detected a peak at 13.2±0.2 Hz with width 4.9±0.3 Hz and rms 1.9±0.5%, but its low (2σ) significance was not compelling.

4. Discussion

Using 600 ksec of new data from the bright LMC binary LMC X–2, we have shown that the source traces out Z-like tracks in the HID and CD, moving continuously along three branches and not jumping instantaneously from one to the next. The pattern, width, and extent of the tracks show particular similarity with those observed from GX 17+2 (e.g. Homan et al. 2002), Sco X–1 (e.g. Dieters & van der Klis 2000), and GX 349+2 (e.g. O'Neill et al. 2002), and have little in common with the simpler atoll source tracks.

By convention, position on the Z is parameterized using the S_z rank number, in which the HB/NB and NB/FB vertices are defined as S_z=1 and S_z=2 respectively, and the rest of the track is scaled according to the length of the NB (e.g. Hasinger et al. 1990; Hertz et al. 1992; Dieters & van der Klis 2000). Adopting this parameterization, we have obtained data from LMC X–2 covering the range $S_z = -1.0$–4.6, a full span equivalent to that seen in the other Z-sources. Our observations show good coverage of all three branches; LMC X–2 spent roughly 30%, 40%, and 30% of the total observing time in the HB ($S_z \leq 1$), NB ($1 < S_z \leq 2$), and FB ($S_z > 2$) respectively.

The power density spectra derived from the three branches of LMC X–2 appear rather featureless when compared to those of the Z sources, or indeed to those of the atoll sources. The spectra are dominated by VLFN, with little significant evidence for either peaked low frequency noise (LFN) at 10–100 Hz, or NBO/FBO. The power law indices and rms amplitudes measured for the VLFN in LMC X–2, and the overall steepening trend of the VLFN when moving from the HB to the FB, are similar to those observed in the Z sources GX 349+2,

Sco X–1, and GX 17+2, with a particularly close match to the relatively flat VLFN indices of γ=0.6–2.0 measured in GX 17+2 data (Kuulkers et al. 1997; Dieters & van der Klis 2000; O'Neill et al. 2001, 2002; Homan et al. 2002). Of course, the power law indices we measure may be artificially low, due to the possibility of 'contamination' by unresolved LFN and HFN components.

On the basis of their timing and spectral behavior, the Galactic Z-sources have been divided into two categories (Hasinger & van der Klis 1989; Penninx et al. 1991; Kuulkers et al. 1994). It has been proposed that the 'Cyg-like' sources, Cyg X–2, GX 5–1, and GX 340+0, have either a higher inclination (Kuulkers, van der Klis & Vaughan 1996) or a higher magnetic field strength (Psaltis, Lamb & Miller 1995) than the 'Sco-like' sources, Sco X–1, GX 17+2, and GX 349+2. Based on the shapes of its HID and CD, and the observation of intensity flares rather than dips in its FB, LMC X–2 falls squarely into the Sco-like category. However, the Cyg-like sources typically show secular variations in the position of the Z of ~5–10% (GX 5–1 – Kuulkers et al. 1994; Cyg X–2 – Kuulkers et al. 1996, Wijnands et al. 1997b; GX340+0 – Kuulkers & van der Klis 1996), while in the Sco-like sources secular changes in the Z are rare, seen only occasionally in one source, GX 17+2 (Wijnands et al 1997a; Homan et al 2002). In this context, the secular shifts of 2.5–10% we observe from LMC X–2 over the course of a year become intriguing. A series of *RXTE* observations is currently under way to provide medium-term monitoring of LMC X–2 to further study the degree and timescale of these secular variations, and perform additional sensitive searches for QPOs.

REFERENCES

Bradt, H. V., Rothschild, R. E., & Swank, J. H. 1993, A&AS, 97, 355

Dieters, S.W., & van der Klis, M. 2000, MNRAS, 311, 201

Hasinger, G., & van der Klis, M. 1989, A&A, 225, 79

Hasinger, G., van der Klis, M., Ebisawa, K., Dotani, T., & Mitsuda, K. 1990, A&A 235, 131

Hertz, P., Vaughan, B., Wood, K. S., Norris, J. P., Mitsuda, K., Michelson, P. F., & Dotani, T. 1992, ApJ, 396, 201

Homan, J., van der Klis, M., Jonker, P. G., Wijnands, R., Kuulkers, E., Méndez, M., & Lewin, W. H. G. 2002, ApJ, 568, 878

Jahoda, K., Swank, J. H., Giles, A. B., Stark, M. J., Strohmayer, T., Zhang, W., & Morgan, E. H. 1996, in EUV, X-ray and Gamma-Ray Instrumentation for Astronomy VII, ed O. H. Siegmund (Bellingham, WA: SPIE), 59

Kuulkers, E., & van der Klis, M. 1996, A&A, 314, 567

Kuulkers, E., van der Klis, M., & Vaughan, B. A. 1996, A&A, 311, 197

Kuulkers, E., van der Klis, M., Oosterbroek, T., Asai, K., Dotani, T., van Paradijs, J., & Lewin, W. H. G. 1994, A&A, 289, 795

Kuulkers, E., van der Klis, M., Oosterbroek, T., van Paradijs, J., & Lewin, W. H. G. 1997, MNRAS, 287, 495

Muno, M. P., Remillard, R. A., & Chakrabarty, D., 2002, ApJ, 568, L35

O'Neill, P. M., Kuulkers, E. Sood, R. K., & Dotani, T., 2001, A&A, 370, 479

O'Neill, P. M., Kuulkers, E. Sood, R. K., & van der Klis, M., 2002, MNRAS, 336, 217

Penninx, W., Lewin, W. H. G., Tan, J., van Paradijs, J., van der Klis, M., & Mitsuda, K., 1991, MNRAS 249, 113

Prins, S., & van der Klis, M., 1997, A&A, 319, 498

Psaltis, D., Lamb, F. K., & Miller, G. S., 1995, ApJ, 454, L137

Shirey, R. E., Bradt, H. V., & Levine, A. M., 1999, ApJ, 517, 472

Shirey, R. E., Bradt, H. V., Levine, A. M., & Morgan, E. H., 1998, ApJ, 506, 374

Smale, A. P., & Kuulkers, E. 2000, ApJ, 528, 702

van der Klis, M. 1995, in X-ray Binaries, W. H. G. Lewin, J. van Paradijs, & E. P. J. van den Heuvel (eds.), Cambridge University Press, 252

Wijnands, R. A. D., Homan, J., van der Klis, M., Mendez, M., Kuulkers, E., van Paradijs, J., Lewin, W.H.G., Lamb, F.K., Psaltis, D., & Vaughan, B., 1997a, ApJ, 490, L157

Wijnands, R. A. D., van der Klis, M., Kuulkers, E., Asai, K., & Hasinger, G. 1997b, A&A, 323, 399

Wijnands, R. A. D., van der Klis, M., Méndez, M., van Paradijs, J., Lewin, W. H. G., Lamb, F. K., Vaughan, B., & Kuulkers, E., 1998, ApJ, 495, L39

This preprint was prepared with the AAS LaTeX macros v5.0.

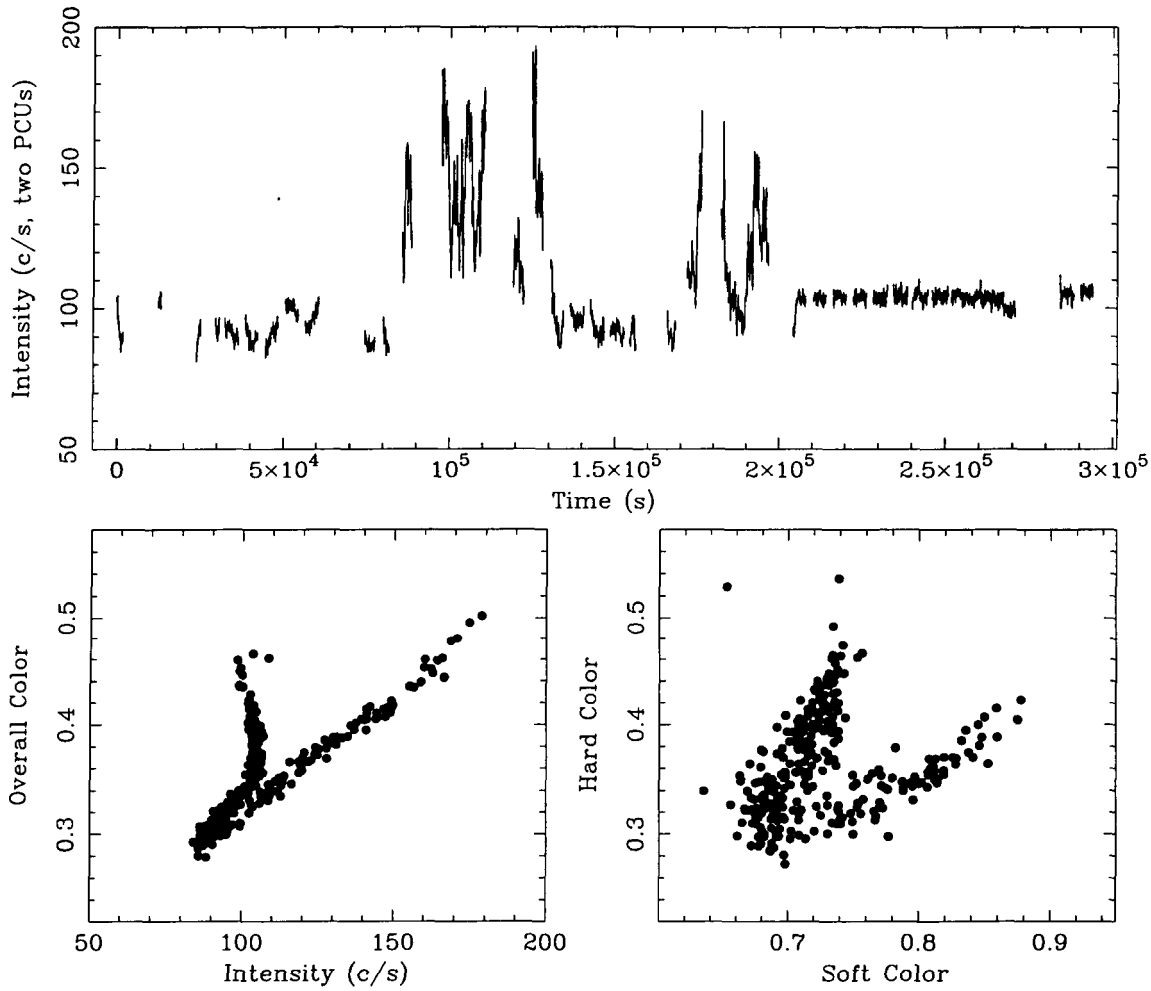

Fig. 1.— *RXTE* PCA light curves, HIDs, and CDs of LMC X–2 obtained during each of the four observations: (a) 2001 February 10–14; (b) 2001 August 30–September 2; (c) 2001 December 13–16; (d) 2002 February 1–6. The definitions of the energy ranges used for the colors can be found in Section 2. The binsize is 128s for the light curve, and 512s for the HID and CD. Data points from the four observations are indicated using filled circles, crosses, squares, and triangles respectively, for easy comparison with Figure 2.

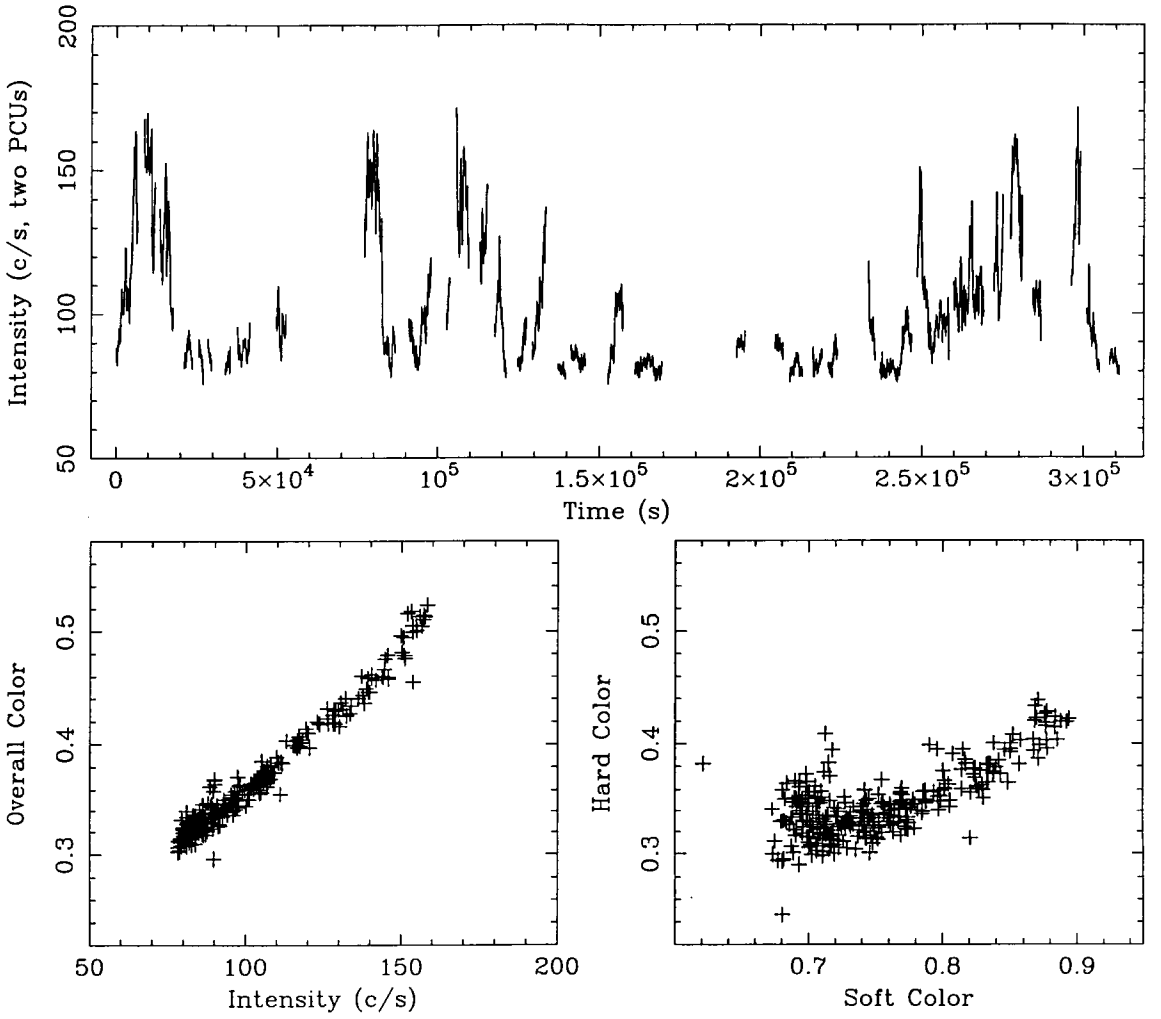
Intensity (c/s, two PCUs)
50
100
150
200
0
5×10^4
10^5
1.5×10^5
2×10^5
2.5×10^5
3×10^5
Time (s)
Overall Color
0.3
0.4
0.5
50
100
150
200
Intensity (c/s)
Hard Color
0.3
0.4
0.5
0.7
0.8
0.9
Soft Color

Fig. 1b.—

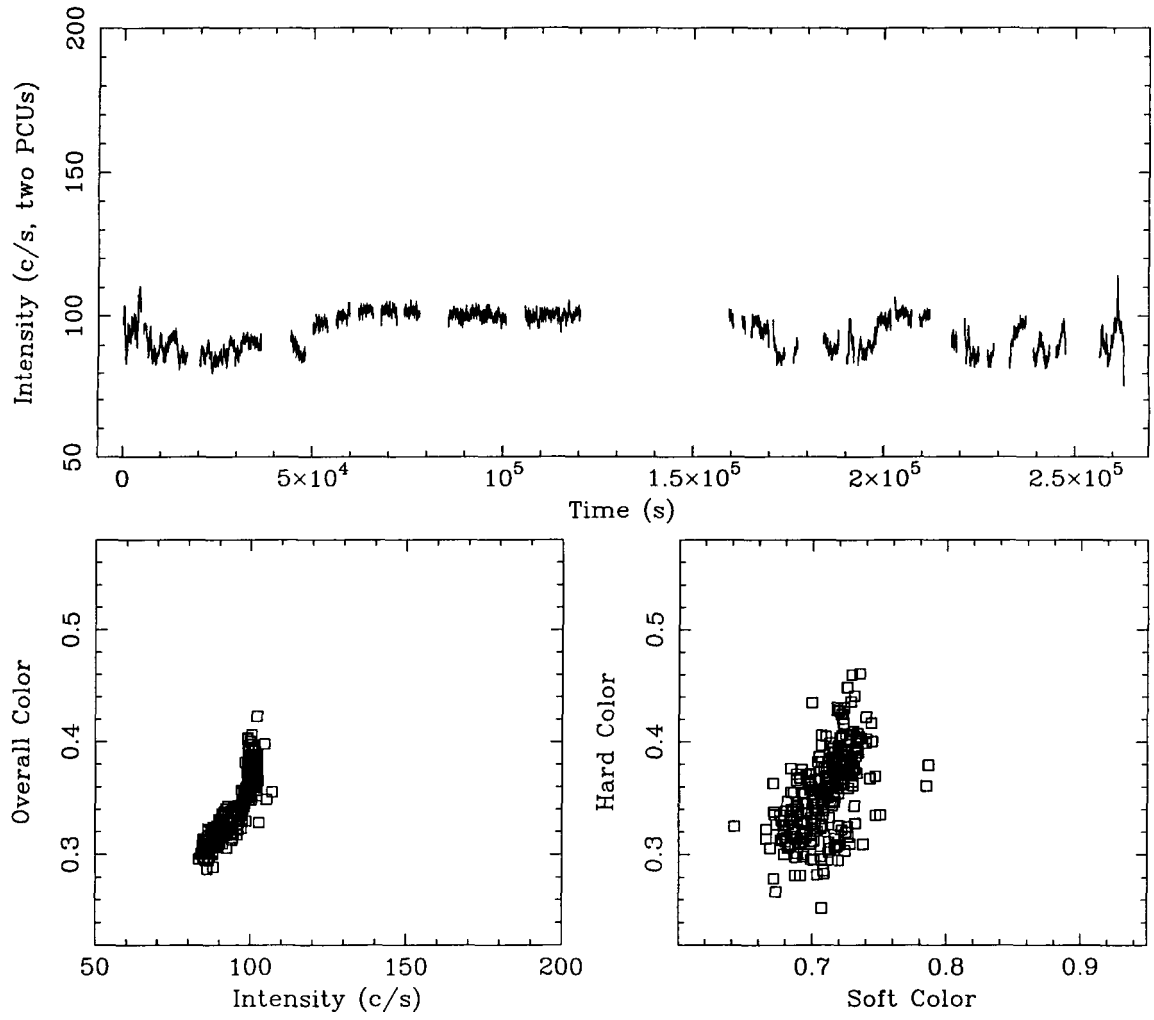
Intensity (c/s, two PCUs)
50
100
150
200
0
5×10^4
10^5
1.5×10^5
2×10^5
2.5×10^5
Time (s)
Overall Color
0.3
0.4
0.5
50
100
150
200
Intensity (c/s)
Hard Color
0.3
0.4
0.5
0.7
0.8
0.9
Soft Color

Fig. 1c.—

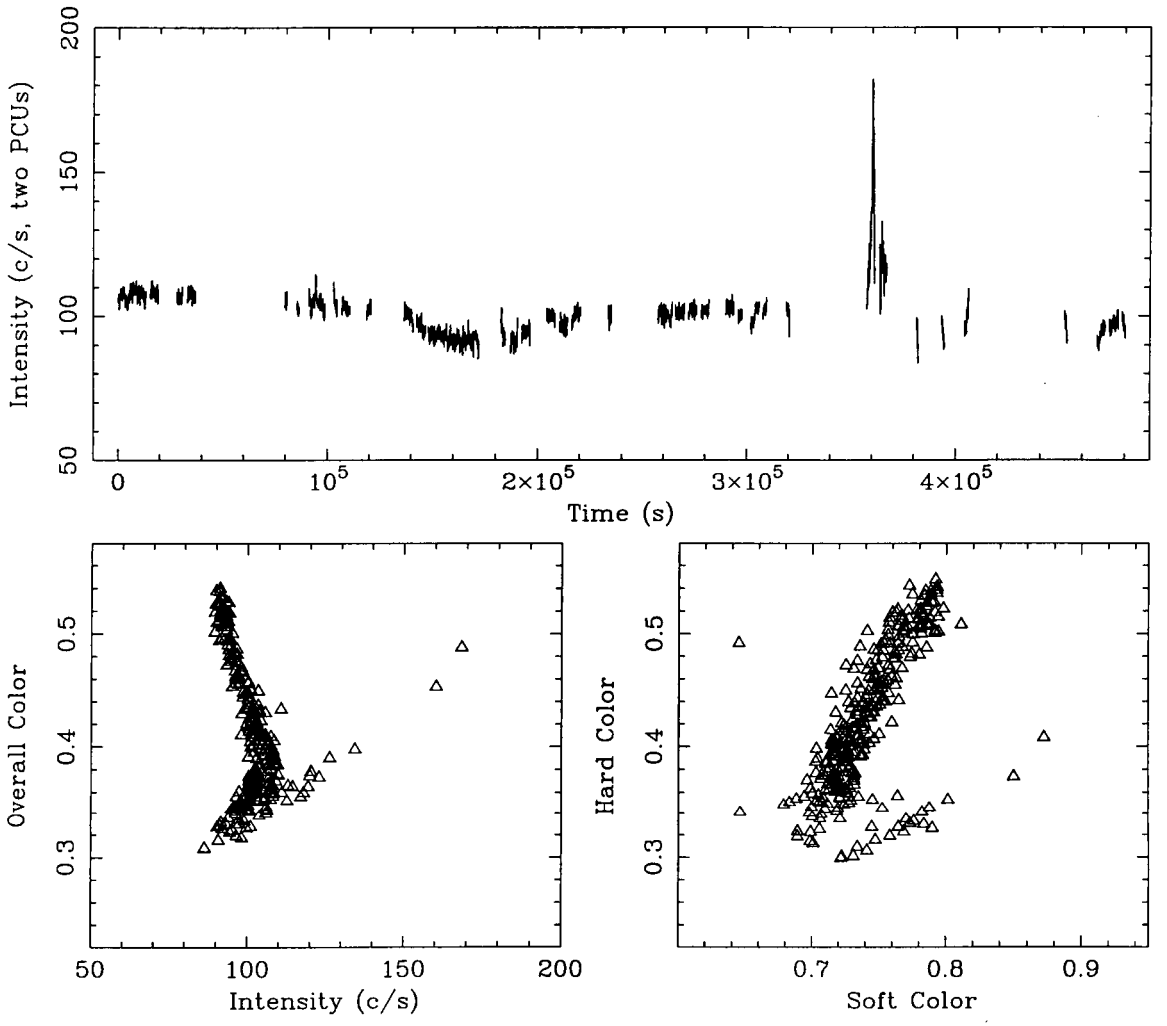
Intensity (c/s, two PCUs)
50
100
150
200
0
10^5
2×10^5
3×10^5
4×10^5
Time (s)
Overall Color
0.3
0.4
0.5
50
100
150
200
Intensity (c/s)
Hard Color
0.3
0.4
0.5
0.7
0.8
0.9
Soft Color

Fig. 1d.—

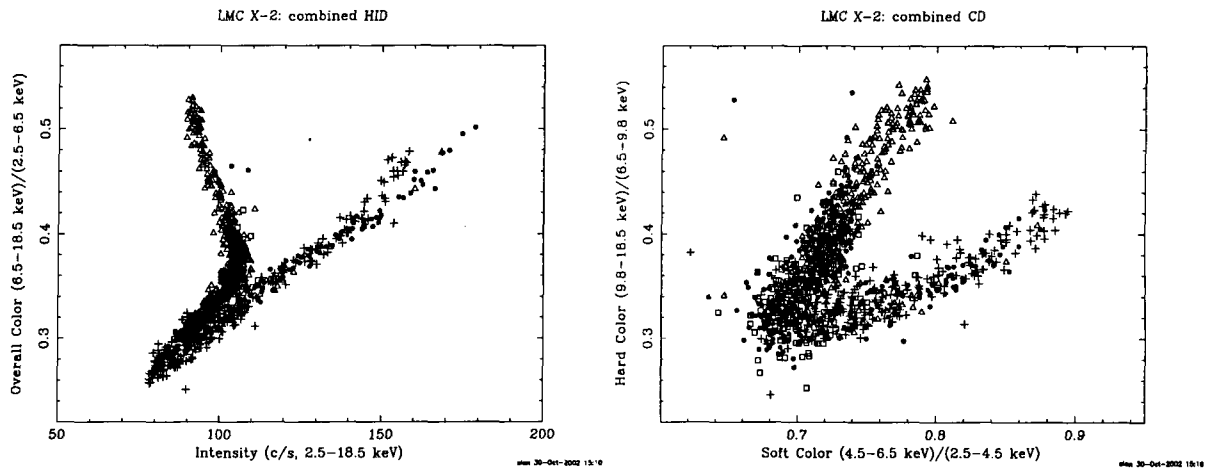

Fig. 2.— Left: Combined HID for all four observations of LMC X–2. Right: Combined CD. Each datapoint represents 512s of data. Data points from each of the four observations are indicated using filled circles, crosses, squares, and triangles respectively, matching the convention in Figure 1.

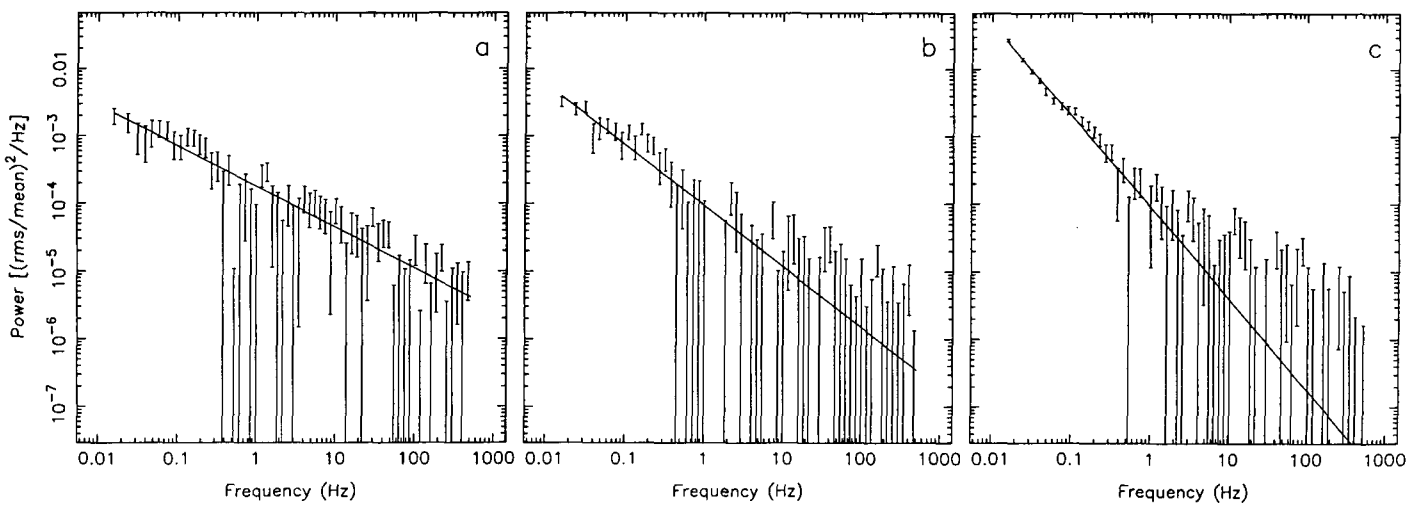

Fig. 3.— Power density spectra of LMC X–2 for the three branches of the Z: (a) Horizontal branch, (b) Normal branch, (c) Flaring branch.